ADVANCED MATERIALS
www.advmat.de

Simultaneous Enhancement of Electrical Conductivity and Thermopower of Bi_2Te_3 by Multifunctionality of Native Defects

*Joonki Suh, Kin Man Yu, Deyi Fu, Xinyu Liu, Fan Yang, Jin Fan, David J. Smith, Yong-Hang Zhang, Jacek K. Furdyna, Chris Dames, Wladyslaw Walukiewicz, and Junqiao Wu**

Thermoelectric materials have been heavily investigated over the past several decades for environment-friendly applications of solid-state energy conversion: heat to electricity and vice versa.[1,2] The figure of merit (ZT) of thermoelectric materials is given by $\alpha^2\sigma T/\kappa$, in which α is the Seebeck coefficient (thermopower), σ is the electrical conductivity, T is absolute temperature, and κ is the thermal conductivity. Since α and σ are anticorrelated through the free carrier concentration (n), recent successes to enhance ZT have mostly relied on reduction of lattice thermal conductivity (κ_l) without significantly affecting the power factor ($\alpha^2\sigma$).[3] This approach has achieved ZT of PbTe–SrTe compounds exceeding 2 at temperatures above 900 K by effectively scattering acoustic phonons with all-length-scale mean free paths.[4]

On the contrary, the best single-phase materials (i.e., excluding superlattices)[5] available today for near-room-temperature thermoelectrics are Bi_2Te_3-based bulk alloys, and their best ZT is still around 1, e.g., n-type $Bi_2Te_{2.7}Se_{0.3}$ with $ZT_{max} \approx 0.9$[6] and p-type $Bi_{0.5}Sb_{1.5}Te_3$ with $ZT_{max} \approx 1.2$.[7] The approach of phonon engineering has limited potential for these materials as their thermal conductivity is already low and does not have much room for further reduction.[5,8] Hence, it is ultimately necessary to seek a breakthrough in materials engineering that would improve ZT beyond what is limited by the trade-off between α and σ, preferably with a single methodology. Though various experimental (e.g., energy filtering in Bi_2Te_3/Bi_2Se_3 superlattices)[9] and theoretical (e.g., hybridization by topological surface states)[10] approaches have been attempted or proposed, only α or σ, but not both, is effectively improved in these cases. The trade-off between α and σ originates fundamentally from the fact that a high α prefers a large asymmetry in electron population above and below the Fermi level, thus a rapid variation in the material density of states; this is opposite to the direction of increasing σ and n, which occurs typically as the Fermi level is displaced deep into the band where the density of states is relatively constant.

Here, we demonstrate a new way to drastically enhance thermoelectric properties of Bi_2Te_3 by utilizing native defects (NDs). We present a new, atomic-scale mechanism to break the trade-off between α and σ, simultaneously improving both for enhanced ZT. Such a unique combination of electrical and thermoelectric benefits originates from the multifunctionality of native point defects in Bi_2Te_3 acting as electron donors and electron energy filters. The presented results establish the importance of understanding and controlling point defects in thermoelectric materials as a venue to much improve their device performance.

Bi_2Te_3 thin films with a wide range of thicknesses (11 nm to 1 μm) were grown by molecular beam epitaxy (MBE) on semi-insulating GaAs (001) substrates. In **Figure 1**a, the cross-section high-resolution transmission electron microscopy (HRTEM) image shows clean interfaces without amorphous phases, and shows highly parallel quintuple layers (QLs). The crystallinity of the MBE films was further evaluated by X-ray diffraction (XRD) using the Cu Kα1 radiation line (Figure 1b). The XRD pattern clearly shows strong reflections from {003}-type lattice planes. This is a strong indication of the highly c-axis directional growth of the MBE films. The QL thickness was calculated from the XRD data, giving d_{QL} = 1.014 ± 0.005 nm for Bi_2Te_3 that is consistent with the value of 1.016 nm for bulk Bi_2Te_3.[11]

J. Suh, Dr. K. M. Yu, Dr. D. Fu, Dr. W. Walukiewicz, Prof. J. Wu
Department of Materials Science and Engineering
University of California
Berkeley, CA 94720, USA
E-mail: wuj@berkeley.edu
J. Suh, Dr. K. M. Yu, Dr. D. Fu, Dr. W. Walukiewicz, Prof. J. Wu
Materials Sciences Division
Lawrence Berkeley National Laboratory
Berkeley, CA 94720, USA
Dr. X. Liu, Prof. J. K. Furdyna
Department of Physics
University of Notre Dame
Notre Dame, IN 46556, USA
Dr. F. Yang, Prof. C. Dames
Department of Mechanical Engineering
University of California
Berkeley, CA 94720, USA
Dr. J. Fan, Prof. D. J. Smith
Department of Physics
Arizona State University
Tempe, AZ 85287, USA
Prof. Y.-H. Zhang
School of Electrical
Computer and Energy Engineering
Arizona State University
Tempe, AZ 85287, USA

DOI: 10.1002/adma.201501350

© 2015 WILEY-VCH Verlag GmbH & Co. KGaA, Weinheim

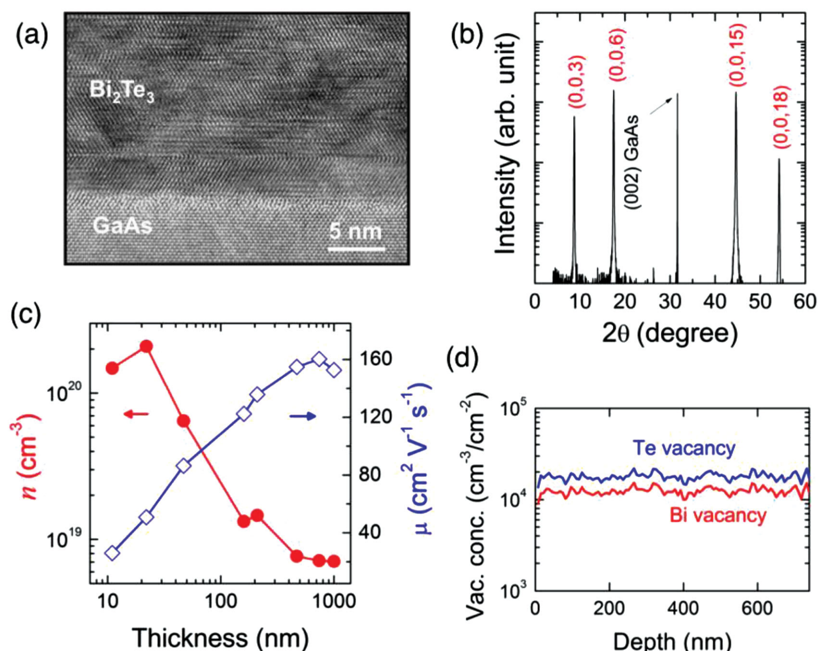

Figure 1. Characterization of pristine Bi_2Te_3 films. a) Cross-sectional HRTEM image and b) XRD data of Bi_2Te_3 films grown by MBE on a GaAs (001) substrate. c) Hall effect determined carrier density and mobility as a function of thickness at room temperature. d) The concentration of vacancies was calculated using SRIM for 740 nm thick Bi_2Te_3 film under 3 MeV alpha particles irradiation. SRIM predicts that the concentration of irradiation-induced defects is very uniform along the depth of films. As indicated by the units (cm^{-3}/cm^{-2}), the real vacancy concentration is given by this value multiplied with the irradiation dose (in units cm^{-2}), implying a linear dependence between them.

Hall effect measurements were performed in the van der Pauw configuration using an Ecopia HMS-3000 system. As presented in Figure 1c, n decreases and carrier mobility (μ) increases monotonically with film thickness, and tends to saturate in thicker films, akin to those observed in Bi_2Se_3 MBE thin films.[12] In order to generate NDs, the samples were irradiated with 3 MeV alpha particles (He^{2+}) with doses ranging from 2×10^{13} to 3×10^{15} cm^{-2}. The projected range of these particles exceeds 8 µm in Bi_2Te_3, as calculated by Monte Carlo simulation using the stopping and range of ions in matter (SRIM) program (Figure S1, Supporting Information, inset). Therefore, the He^{2+} ions completely pass through the entire film thickness, leaving behind NDs that are uniformly distributed in both lateral and depth directions. As predicted by SRIM, the primary NDs induced by irradiation are Bi (V_{Bi}) and Te (V_{Te}) vacancies and corresponding interstitials with average densities of 1.2×10^4 (for Bi) and 1.8×10^4 cm^{-3}/ion cm^{-2} (for Te), respectively, that scale linearly with the irradiation dose (Figure 1d). We note that within the doses used, the materials are gently damaged with only point defects generated; no extended defects, surface sputtering, non-stoichiometry, or amorphization is observed.[13] We also note that the substrate (semi-insulating GaAs) does not contribute to the electrical conductivity measured from the film. It is theoretically expected[14] and experimentally confirmed that the substrate remains electrically extremely insulating after the irradiation, with a sheet resistance orders of magnitude higher than that of the film.

After the irradiation, σ of the Bi_2Te_3 increases for films with thickness between 47 and 740 nm, and this trend is more significant for thicker films (**Figure 2**a). Considering the multiple conduction channels (e.g., surface and bulk) in Bi_2Te_3, this effect suggests that bulk transport, which is affected by the NDs, plays an important role in the electrical conductance in this thickness range. In contrast, very thin films are insensitive to irradiation, because surface conduction dominates and remains robust to irradiation. Hall effect measurements reveal that the enhanced σ is a combined effect of a monotonic increase in n and a non-monotonic change of μ (Figure 2b,c). The increase in n indicates that the irradiation predominantly introduces donor-like NDs, which are also considered as the primary reason for the unintentional n-type behavior of as-prepared Bi_2Te_3.[15,16]

As shown in Figure 2c, the mobility of thick films increases remarkably (by up to 50%) upon irradiation until an intermediate dose (≈2×10^{14} cm^{-2}), then steadily decreases. For

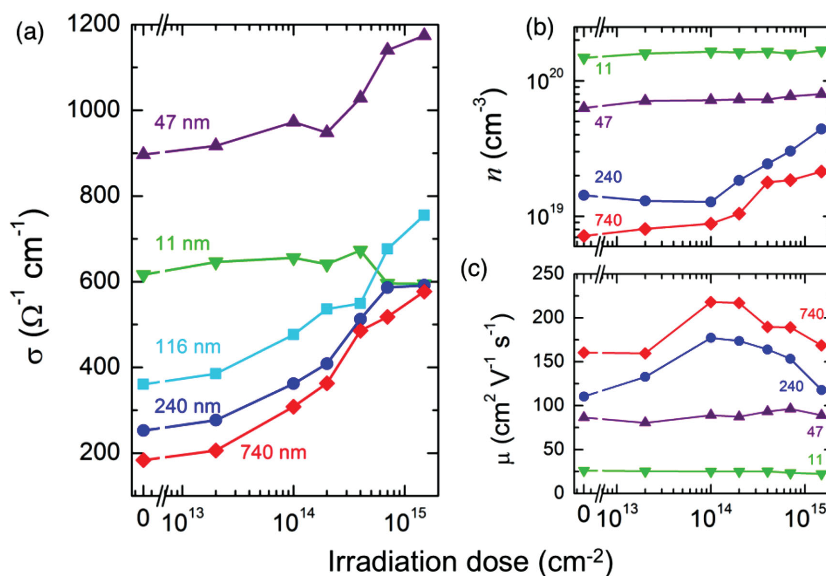

Figure 2. Electrical transport of ND-engineered Bi_2Te_3 thin films. a) Electrical conductivity variation upon irradiation of films with different thicknesses. b) Electron concentration and c) electron mobility of representative Bi_2Te_3 films as a function of irradiation dose, determined by Hall effect measurement at room temperature.

© 2015 WILEY-VCH Verlag GmbH & Co. KGaA, Weinheim

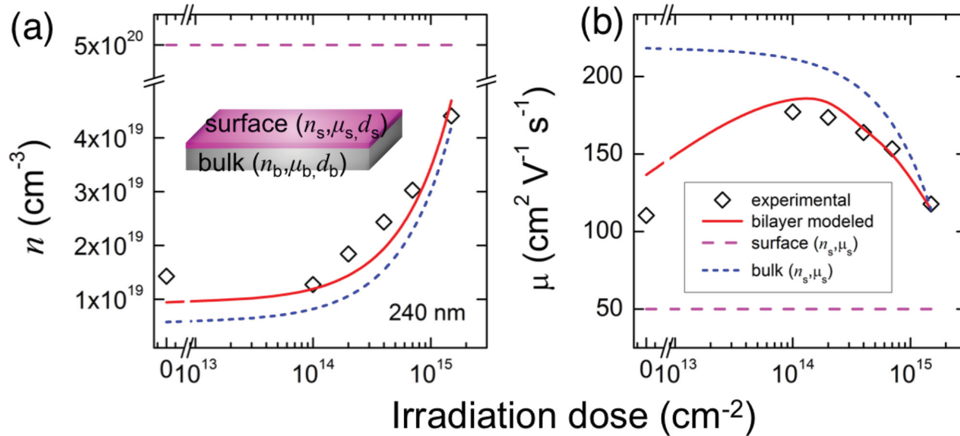

Figure 3. Bilayer Hall effect modeling of Bi_2Te_3 films. Comparison of a) electron concentration and b) electron mobility between experimental data with bilayer modeled data for 240 nm film. Inset shows schematics of the two conduction channels of surface and bulk. Surface properties are assumed to be constant for all the films within the ranges of thickness and irradiation dose. Also, its thickness (d_s) is assumed to be ≈3 nm, considering other contributions such as grain boundaries in the bulk as well as the surface roughness.

conventional semiconductors, it is believed that NDs produced by irradiation are charged Coulomb scattering centers, lowering the carrier relaxation time and thus the carrier mobility. Recent theoretical and experimental studies have shown that in addition to the bulk transport, Bi_2Te_3 exhibits significant surface or grain boundary transport, which are attributed to the topological insulator state[17] or to a surface accumulation layer.[18,19] We propose that the irradiation-induced NDs cause the unusual mobility behavior of Figure 2c by modifying the relative contribution of conduction electrons between the bulk and the surface (including grain boundaries and specimen surface). Simplifying the system into two electrically conduction channels, surface and bulk, we modeled the dependence of carrier concentration and mobility on irradiation dose.[20,21] As illustrated in the inset of **Figure 3**a, parallel electron transport was considered in the surface and bulk layers. With the relative contribution from each layer, effective (modeled) electron concentration (n^*) and mobility (μ^*) were determined using:

$$n^* = \frac{\left[n_s\mu_s(d_s/d) + n_b\mu_b(d_b/d)\right]^2}{n_s\mu_s^2(d_s/d) + n_b\mu_b^2(d_b/d)} \tag{1}$$

$$\mu^* = \frac{n_s\mu_s^2(d_s/d) + n_b\mu_b^2(d_b/d)}{n_s\mu_s(d_s/d) + n_b\mu_b(d_b/d)} \tag{2}$$

where $n_s(n_b)$ and $\mu_s(\mu_b)$ are the electron concentration and mobility of surface (bulk) layer, respectively, and $d_s(d_b)$ is the thickness of surface (bulk) layer, and the total thickness, d, is given by $d = d_s + d_b$.[20] The surface properties (n_s and μ_s) are inferred from Hall effect data of very thin films (11–22 nm) where surface contribution is dominant. Note that in this model n_s and μ_s are assumed to be not strongly affected by irradiation, i.e., the irradiation generates more free electrons only in the bulk (increasing net n_b), as opposed to redistributing existing surface n_s to the bulk n_b. Indeed, in very thin films where the bulk conduction is insignificant, the measured n^* (Hall μ^*) is always dominated by n_s (μ_s), staying high (low) and nearly intact upon irradiation (Figure 2b,c). Given that μ_s is insensitive to the irradiation and $\mu_s \ll \mu_b$,[13,22] n^* and μ^* were fitted to the experimental Hall effect data at various irradiation doses. Such a bilayer model is in good agreement with the experimental data for films with various thicknesses, explaining both the monotonically increasing n^* and, in particular, non-monotonic variation of μ^* upon irradiation (see representative fitting in Figure 3). The irradiation-induced, drastic net increase in bulk electron density would shift the weight more toward bulk conduction, compared to the case in pristine films where surface conduction weighs more. Therefore, although μ_b slightly decreases upon irradiation, the measured μ^* shows an increase at intermediate irradiation doses, because after irradiation the higher-mobility bulk conduction plays a much more significant role than the surface conduction.

More importantly, while steadily increasing σ, the NDs at intermediate irradiation doses also improve the thermopower (α) of the thick Bi_2Te_3 films as seen in **Figure 4**a. This simultaneous enhancement of α and σ is unusual, since in most cases α decreases and σ increases with increasing n. Normally, as n increases, the Fermi level ε_F moves deeper into the band where the density of states is flatter, hence reducing the entropy carried by charges around ε_F.[23] The simultaneous enhancement of α and σ is observed only in relatively thicker films (>47 nm), which suggests that the measured thermopower is dominated by the bulk contribution that can be tailored by the NDs.

In the relaxation time model, the thermopower in the degenerate doping limit is given by:

$$|\alpha| \approx \frac{k_B}{e}\cdot\frac{\pi^2}{3}\cdot\frac{k_B T}{\varepsilon_F}\cdot\left(\frac{3}{2}+r\right) \tag{3}$$

where r is the index of the electron relaxation time related to kinetic energy, $\tau(\varepsilon) \propto \varepsilon^r$,[24] and ε_F is measured from the conduction band edge. Equation (3) not only predicts the ordinary decrease in α as n increases (through ε_F), but also an increase in α when r increases. The former leads to the conventional wisdom of the inverse coupling between α and σ, while the latter allows it to be broken, as in our case. It is known that r varies from −1/2 for acoustic phonon scattering to 3/2 for ionized impurity scattering.[24] As shown in Figure 4b, in pristine

© 2015 WILEY-VCH Verlag GmbH & Co. KGaA, Weinheim

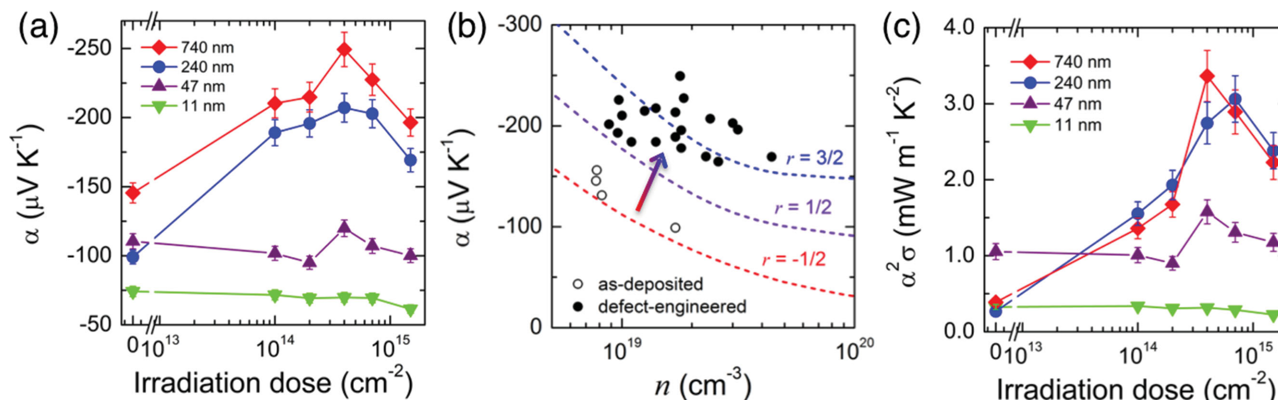

Figure 4. Enhancement of Seebeck coefficient and power factor by the NDs. a) Variation of α upon irradiation. b) α enhancement of irradiated Bi_2Te_3 films in the thick film regime (Pisarenko plot). The dotted lines show the results of calculated Seebeck coefficient with different scattering time index r ranging from phonon-scattering (–1/2) to ionized impurity scattering (3/2). Here, the rigorous Fermi–Dirac carrier statistics are used such that the calculation is valid across all concentrations ranging from non-degenerate to degenerate. The arrow indicates simultaneous increase of α and carrier concentration (n) of the films. c) Thermoelectric power factor enhancement in the ND-engineered Bi_2Te_3 films.

films, the measured α as a function of n follows the trend with calculation using $r = -1/2$, indicating that electrons are mostly scattered by phonons in these films. This is consistent with theoretical prediction that electrical transport in Bi_2Te_3 at similar carrier concentrations ($\approx 1 \times 10^{19}$ cm^{-3}) is limited by phonon scattering,[25] and is indeed reasonable considering its very large dielectric constant ($\varepsilon_s = 290$).[26] However, the high density and multiple charge states of NDs introduced by irradiation as ionized impurities cause a transition of the scattering mechanism from phonon-dominated ($r = -1/2$) toward more impurity-dominated ($r = 3/2$); as a result, the thermopower is drastically enhanced, as indicated by the arrows in Figure 4b. For the irradiated films, α starts to follow the calculated trend with $r = 3/2$. This transition is also confirmed by the fact that the mobility μ of the pristine film becomes much higher when measured at low temperatures, while μ is less temperature-sensitive for irradiated films (Figure S1, Supporting Information).

The ND-enabled decoupling of α and σ naturally leads to a significant increase in the thermoelectric power factor, $\alpha^2\sigma$, as shown in Figure 4c. It reaches a peak value of 3.4 ± 0.3 mW m^{-1} K^{-2} for the 740 nm film at an irradiation dose of 4×10^{14} cm^{-2}, representing an eightfold enhancement from its pristine value. This peak power factor is a factor of 1.5–3 higher compared to recently reported values in binary Bi_2Te_3.[9,27]

In addition, the effect of the NDs on the cross-plane (c-axis) thermal conductivity ($\kappa_\perp$), particularly in the thick Bi_2Te_3 films, was investigated using the differential 3ω technique.[28] We found that $\kappa_\perp$ decreases by up to 35% upon the irradiation as shown in **Figure 5**. It is noteworthy that the reduction in $\kappa_\perp$ is substantially stronger than the case if the NDs were replaced by conventional donor ions at the same concentrations ($\approx 3 \times 10^{19}$ cm^{-3}, or ≈0.1% of the atomic sites). This is because a point defect's ability to scatter acoustic phonons goes as the square of the defect's relative deviation in mass, radius, and/or bonding strength.[29] These relative deviations are much stronger for the irradiation-introduced NDs (vacancies, antisites, and missing bonds) as compared to simple substitutional dopants.[30] As our measured κ is cross-plane (⊥), while the measured α and σ are in-plane (//), a rigorous evaluation of ZT is not within the scope of this work due to the anisotropic transport. However, given the eightfold enhancement in $\alpha^2\sigma$, it is safe to conclude that ZT is expected to be significantly enhanced accordingly, because κ is expected to only decrease upon the irradiation.

To summarize, irradiation-induced NDs drastically enhance thermoelectric properties in Bi_2Te_3 by decoupling the three key thermoelectric parameters and simultaneously modifying all of them toward the desired direction. This is enabled by the multiple functionality of the NDs acting beneficially as electron donors, energy-dependent charge scattering centers, and phonon blockers. Our results suggest that a significant improvement of the thermoelectric performance can

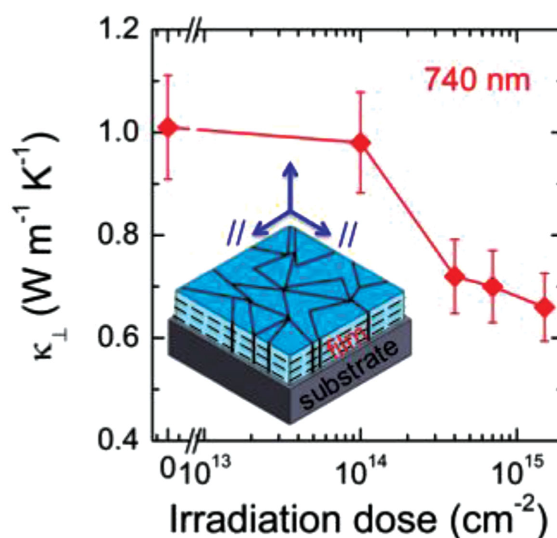

Figure 5. Cross-plane thermal conductivity of the 740 nm Bi_2Te_3 film upon irradiation. Inset illustrates the in-plane and cross-plane configuration of the textured film.

© 2015 WILEY-VCH Verlag GmbH & Co. KGaA, Weinheim

be achieved through a judicious control of the ND species and their density by post-growth processing with high-energy beams. As the NDs are expected to be generated and behave in the similar way in a wide range of narrow-bandgap semiconductors (e.g., observed in InN and InAs)[31,32] it is possible to extend this method to improve the figure of merit of other materials in conjunction with other widely utilized techniques such as alloying and nano- and hetero-structuring. Although irradiation cannot be directly applied to bulk materials due to limitation in irradiation projection range (≈10 µm), our approach is of practical importance because thin film thermoelectrics could play an important role in on-chip cooling;[33] in addition, our approach can be used in complementary to existing nanotechnology to scale up in bulk thermoelectrics. For instance, nano-objects (such as Bi_2Te_3 nanowires, particles, and nanoplates) can be irradiated, and then pressed into bulk or assembled into bulk using a polymer matrix, as demonstrated by Coates et al.[34]

Experimental Section

Thin-Film Growth: The Bi_2Te_3 thin films were grown using a dual chamber Riber 32 solid-source MBE system. The Bi and Te_2 fluxes were generated by standard effusion cells, and the structure and thickness of the films were monitored in situ by reflection high-energy electron diffraction. The growth step was initiated by heating an epi-ready semi-insulating GaAs (001) substrate to 600 °C for de-oxidation in the III-V MBE chamber. This was followed by deposition of a 100 nm GaAs buffer layer. This modified substrate was then transferred to the chalcogenide MBE chamber through an ultra-high vacuum connection. The growth of the MBE film was initiated by the deposition of a series of monolayers of Te–Bi–Te–Bi–Te (a QL) in atomic layer epitaxy fashion at room temperature. The substrate was then gradually heated to 300 °C, and the MBE growth of Bi_2Te_3 was subsequently performed under Te-rich condition of T_{Te} (250 °C) < $T_{substrate}$ (300 °C) < T_{Bi} (≈500 °C) with a Te:Bi beam equivalent pressure ratio ranging from 20:1 to 80:1. The films were grown layer by layer, with typical growth rates of 0.5–2 QL min^{-1}. Later, the compositions and thicknesses of the films were confirmed by Rutherford backscattering spectroscopy (RBS) before further experiments.

Alpha Particle Irradiation: The pristine samples were irradiated in an accumulated manner employing a high-energy (3 MeV) He^{2+} beam with current between 35 and 100 nA generated by an NEC Pelletron tandem accelerator. The accumulated dose was monitored by measuring the total charge on the sample in an electrically isolated irradiation chamber. The ion beam was defocused to an area of 40 mm^2 maintaining a homogeneous ion fluence over the entire film, assuring the introduction of uniformly distributed NDs, both vertically and laterally.

Thermoelectric Transport Characterization: Electrical transport was measured by Hall effect using an Ecopia HMS-3000 system at room temperature. Seebeck coefficient was measured by a home-built thermopower measurement system. A differential 3ω technique was used to measure the cross-sectional thermal conductivity ($\kappa_\perp$) of the ND-engineered Bi_2Te_3 thin film with a thickness of 740 nm at various irradiation doses. Using the plasma-enhanced chemical vapor deposition (PECVD) technique, a 500 nm SiO_2 layer was simultaneously deposited on the top of both a pristine Bi_2Te_3 thin film, for electrical isolation, and a reference (identical semi-insulating GaAs (001)) bare substrate at 300 °C. Two identical 20 µm × 1500 µm gold line heaters were then patterned on the top of PECVD-grown SiO_2 layers using conventional photolithography. Since the thicknesses of the dielectric layer (500 nm) and Bi_2Te_3 film (740 nm) are much thinner than the width of the patterned gold heater (20 µm), the through-thickness (along *c*-axis) heat conduction can be approximated as 1D to better than 5% accuracy.[35]

Supporting Information

Supporting Information is available from the Wiley Online Library or from the author.

Acknowledgements

This work was supported by a NSF CAREER Award under Grant No. DMR-1055938. The irradiation and Hall effect parts were supported by the Office of Science, Office of Basic Energy Sciences, of the U.S. Department of Energy under Contract No. DE-AC02-05CH11231. The film growth of Bi_2Te_3 thin films were supported by NSF Grant No. DMR10-05851, NSF Grant No. ECCS10-02114, and an AFOSR Grant No. FA9550-10-1-0129. The authors acknowledge use of facilities in the John M. Cowley Center for High Resolution Electron Microscopy at Arizona State University. The authors wish to thank Prof. Renkun Chen, Prof. Jae Hun Seol, Sean Lubner, Jason Chee, and Chun-Hao Huang for valuable discussions and technical support.

Received: March 20, 2015
Revised: April 20, 2015
Published online: May 12, 2015

[1] S. Chu, A. Majumdar, *Nature* **2012**, *488*, 294.
[2] C. J. Vineis, A. Shakouri, A. Majumdar, M. G. Kanatzidis, *Adv. Mater.* **2010**, *22*, 3970.
[3] A. Shakouri, *Annu. Rev. Mater. Res.* **2011**, *41*, 399.
[4] K. Biswas, J. He, I. D. Blum, C.-I. Wu, T. P. Hogan, D. N. Seidman, V. P. Dravid, M. G. Kanatzidis, *Nature* **2012**, *489*, 414.
[5] R. Venkatasubramanian, E. Siivola, T. Colpitts, B. O'Quinn, *Nature* **2001**, *413*, 597.
[6] X. Yan, B. Poudel, Y. Ma, W. S. Liu, G. Joshi, H. Wang, Y. Lan, D. Wang, G. Chen, Z. F. Ren, *Nano Lett.* **2010**, *10*, 3373.
[7] B. Poudel, Q. Hao, Y. Ma, Y. Lan, A. Minnich, B. Yu, X. Yan, D. Wang, A. Muto, D. Vashaee, X. Chen, J. Liu, M. S. Dresselhaus, G. Chen, Z. Ren, *Science* **2008**, *320*, 634.
[8] J. P. Fleurial, L. Gailliard, R. Triboulet, H. Scherrer, S. Scherrer, *J. Phys. Chem. Sol.* **1988**, *49*, 1237.
[9] Y. Min, J. W. Roh, H. Yang, M. Park, S. I. Kim, S. Hwang, S. M. Lee, K. H. Lee, U. Jeong, *Adv. Mater.* **2013**, *25*, 1425.
[10] P. Ghaemi, R. S. K. Mong, J. E. Moore, *Phys. Rev. Lett.* **2010**, *105*, 166603.
[11] J. O. Jenkins, J. A. Rayne, R. W. Ure, *Phys. Rev. B* **1972**, *5*, 3171.
[12] Y. S. Kim, M. Brahlek, N. Bansal, E. Edrey, G. A. Kapilevich, K. Iida, M. Tanimura, Y. Horibe, S.-W. Cheong, S. Oh, *Phys. Rev. B* **2011**, *84*, 073109.
[13] J. Suh, D. Fu, X. Liu, J. K. Furdyna, K. M. Yu, W. Walukiewicz, J. Wu, *Phys. Rev. B* **2014**, *89*, 115307.
[14] W. Walukiewicz, *Phys. Rev. B* **1988**, *37*, 4760.
[15] D. O. Scanlon, P. D. C. King, R. P. Singh, A. de la Torre, S. M. Walker, G. Balakrishnan, F. Baumberger, C. R. A. Catlow, *Adv. Mater.* **2012**, *24*, 2154.
[16] D. West, Y. Y. Sun, H. Wang, J. Bang, S. B. Zhang, *Phys. Rev. B* **2012**, *86*, 121201(R).
[17] Y. L. Chen, J. G. Analytis, J.-H. Chu, Z. K. Liu, S.-K. Mo, X. L. Qi, H. J. Zhang, D. H. Lu, X. Dai, Z. Fang, S. C. Zhang, I. R. Fisher, Z. Hussain, Z.-X. Shen, *Science* **2009**, *325*, 178.
[18] C. Chen, S. He, H. Weng, W. Zhang, L. Zhao, H. Liu, X. Jia, D. Mou, S. Liu, J. He, Y. Peng, Y. Feng, Z. Xie, G. Liu, X. Dong, J. Zhang, X. Wang, Q. Peng, Z. Wang, S. Zhang, F. Yang, C. Chen, Z. Xu,

© 2015 WILEY-VCH Verlag GmbH & Co. KGaA, Weinheim

X. Dai, Z. Fang, X. J. Zhou, *Proc. Natl. Acad. Sci. USA* **2012**, *109*, 3694.
[19] M. S. Bahramy, P. D. C. King, A. de la Torre, J. Chang, M. Shi, L. Patthey, G. Balakrishnan, Ph. Hofmann, R. Arita, N. Nagaosa, F. Baumberger, *Nat. Commun.* **2012**, *3*, 1159.
[20] R. L. Petritz, *Phys. Rev.* **1958**, *110*, 1254.
[21] R. E. Jones, K. M. Yu, S. X. Li, W. Walukiewicz, J. W. Ager, E. E. Haller, H. Lu, W. J. Schaff, *Phys. Rev. Lett.* **2006**, *96*, 125505.
[22] N. P. Butch, K. Kirshenbaum, P. Syers, A. B. Sushkov, G. S. Jenkins, H. D. Drew, J. Paglione, *Phys. Rev. B* **2010**, *81*, 241301.
[23] H. J. Goldsmid, *Introduction to Thermoelectricity*, Springer, Heidelberg, Germany **2010**.
[24] F. D. Rosi, *Solid-State Electron.* **1968**, *11*, 833.
[25] B.-L. Huang, M. Kaviany, *Phys. Rev. B* **2008**, *77*, 125209.
[26] W. Richter, H. Kohler, C. R. Becker, *Phys. Status Solidi B* **1977**, *84*, 619.
[27] L. Hu, H. Gao, X. Liu, H. Xie, J. Shen, T. Zhu, X. Zhao, *J. Mater. Chem.* **2012**, *22*, 16484.
[28] C. Dames, G. Chen, *Rev. Sci. Instrum.* **2005**, *76*, 124902.
[29] P. G. Klemens, *Proc. Phys. Soc. A* **1955**, *68*, 1113.
[30] A. X. Levander, T. Tong, K. M. Yu, J. Suh, D. Fu, R. Zhang, H. Lu, W. J. Schaff, O. Dubon, W. Walukiewicz, D. G. Cahill, J. Wu, *Appl. Phys. Lett.* **2011**, *98*, 012108.
[31] J. Wu, W. Walukiewicz, K. M. Yu, W. Shan, J. W. Ager, E. E. Haller, H. Lu, W. J. Schaff, W. K. Metzger, S. Kurtz, *J. Appl. Phys.* **2003**, *94*, 6477.
[32] V. N. Brudnyi, N. G. Kolin, A. I. Potapov, *Semiconductors* **2003**, *37*, 390.
[33] I. Chowdhury, R. Prasher, K. Lofgreen, G. Chrysler, S. Narasimhan, R. Mahajan, D. Koester, R. Alley, R. Venkatasubramanian, *Nat. Nanotechnol.* **2009**, *4*, 235.
[34] N. E. Coates, S. K. Yee, B. McCulloch, K. C. See, A. Majumdar, R. A. Segalman, J. J. Urban, *Adv. Mater.* **2013**, *25*, 1629.
[35] T. Borca-Tasciuc, A. R. Kumar, G. Chen, *Rev. Sci. Instrum.* **2001**, *72*, 2139.

© 2015 WILEY-VCH Verlag GmbH & Co. KGaA, Weinheim